National Aeronautics and Space Administration


# Modeling the Effects of Hydrogen and Dose Rate Sensitivity in CMOS and Bipolar Technologies

Philippe Adell
Jet Propulsion Laboratory
Pasadena, California

Ivan Sanchez
Hugh Barnaby
Arizona State University

Jet Propulsion Laboratory
California Institute of Technology
Pasadena, California

JPL Publication 11-17 12/11

National Aeronautics and Space Administration


# Modeling the Effects of Hydrogen and Dose Rate Sensitivity in CMOS and Bipolar Technologies

NASA Electronic Parts and Packaging (NEPP) Program
Office of Safety and Mission Assurance

Philippe Adell
Jet Propulsion Laboratory
Pasadena, California

Ivan Sanchez
Hugh Barnaby
Arizona State University

NASA WBS: 724297.40.49.11
JPL Project Number: 104593
Task Number: 40.49.03.05

Jet Propulsion Laboratory
4800 Oak Grove Drive
Pasadena, CA 91109

http://nepp.nasa.gov

This research was carried out at the Jet Propulsion Laboratory, California Institute of Technology, and was sponsored by the National Aeronautics and Space Administration Electronic Parts and Packaging (NEPP) Program.

Reference herein to any specific commercial product, process, or service by trade name, trademark, manufacturer, or otherwise, does not constitute or imply its endorsement by the United States Government or the Jet Propulsion Laboratory, California Institute of Technology.

Copyright 2011. California Institute of Technology. Government sponsorship acknowledged.

## TABLE OF CONTENTS

## Abstract

Low dose rate (LDR) and high dose rate (HDR) experiments on field-oxide-field-effect-transistors (FOXFETs) and gated lateral PNP (GLPNP) bipolar transistors indicate that there is a dose rate enhancement factor (EF) associated with radiation-induced degradation. This EF is also affected by the presence of hydrogen in the oxide.

In this work, we developed a one-dimensional (1-D) numerical calculations code to investigate the key mechanisms that describe the dose rate sensitivity and the effect of hydrogen on dose rate effects. We used a finite-difference methodology for the numerical calculations that allows for computing solutions for the densities of the mobile species as well as for the electrostatic potential at nodes contained within a mesh superimposed on the solution domain. Results from calculations of damage to EF indicate that oxide thickness, distribution of hole traps and hole capture cross-section all affect dose rate sensitivity. In addition, calculations show that molecular hydrogen cracking at positively charged defects may be a key reaction relating to hydrogen and dose rate response. Comparison to experimental data on bipolar and complementary metal-oxide semiconductor (CMOS) devices results in good agreement with the dose rate calculations of interface trap buildup.

## 1.0 INTRODUCTION

Total dose and dose rate effects in $SiO_2$-based devices, such as bipolar and CMOS technologies, have been studied extensively. Bipolar transistors and linear circuits are known to exhibit more degradation at low dose rate; this phenomenon is called enhanced low dose rate sensitivity (ELDRS), and was first reported by Enlow *et al*. in 1991 [1]. Since then, different models have been proposed to explain ELDRS. These models can typically be separated into two different types. The first type is a space charge model that focuses on the dose rate dependent effect of positive charge (e.g., trapped holes) on the transport of protons towards the interface [2-4]. The second type of model is based on bimolecular reactions that describe a reduction of proton density in the oxide during high dose rate (HDR) exposures [5, 6]. The combined effect of the mechanisms described by these two models yields an enhancement in interface trap buildup at low dose rate when compared to HDR irradiations. On the other hand, CMOS technologies are generally considered less susceptible to ELDRS compared to bipolar technologies due to the higher electric fields in the oxide regions [7]. However, thick isolation oxides, such as shallow trench isolation (STI) oxides used in advanced CMOS technologies, result in lower fields and can lead to dose rate sensitivity. Recent studies have shown some dose rate effects in advanced CMOS technologies where higher levels of edge leakage in n-channel devices exposed at LDR were observed [8, 9]. This enhancement in degradation was attributed to the dose rate dependent buildup of trapped charge (holes) near the corner of the trench [8]. As described in [8], several factors contribute to the dose rate dependence: 1) low-field recombination could be reduced at LDR due to the lower density of holes produced by radiation (i.e., higher charge yield at LDR) leading to higher degradation, 2) asymmetric field lines along the sidewall and in the corner of the STI leading to a non-uniform buildup of charge along the interface as a function of time, and 3) recombination mechanisms acting upon charge confined within the STI oxide at high dose rates (HDR).

In this work, we developed a generalized 1-D model that simulates the physical mechanisms that contribute to the buildup of defects in $SiO_2$ structures following exposure to ionizing radiation. This model intends to capture both dose rate effects and the impact of hydrogen contamination on the dose rate response. It incorporates hole trapping mechanisms as well as the formation of interface traps due to the release of hydrogen as described by the two-stage hydrogen model [10]. Dose rate effects are simulated following the approach described by Hjalmarson *et al*. in [6], which adopts most of the formalisms presented in [11-13]. The influence of molecular hydrogen on dose rate response is incorporated by using the key reactions that include molecular hydrogen ($H_2$) cracking at positively charged defects and other bimolecular reactions. We will see that modeling results show that space charge effects arise naturally from these bimolecular reactions. As a result, the model therefore captures the combined effect of the two dose rate mechanisms described above. We will show that the dose rate effects in silicon dioxide ($SiO_2$) technologies can be analyzed and modeled by processes that utilize kinetic equations of those mechanisms. Numerical calculations are obtained through a finite difference representation of the model.

To support this model, we present data from dose rate experiments on both field-oxide-field-effect-transistors (FOXFETs) fabricated in a commercial 90-nm CMOS technology and gated lateral pnp bipolar transistors from the national semiconductor (NSC) process. For both device types, we used their electrical characteristics to extract the densities of radiation-induced defects (i.e., oxide trap charge, $N_{ot}$, and interface trap, $N_{it}$). The 1-D model is used to compare the dose rate sensitivity of both structures and investigate the mechanisms that contribute to the dose rate dependent buildup of these defects. Finally, we discuss the calculation results and provide insight into the key factors that determine total dose and dose rate effects in these technologies. Results indicate that the influence of different parameters, such as applied bias, dose-rate, hydrogen contamination and distribution of trapping precursors (i.e., processing defects) all can affect the dose and dose rate response of $SiO_2$ devices.

## 2.0 1-D MODEL

In this section we present a theoretical model that describes the physical mechanisms contributing to the buildup of radiation-induced defects in a MOS system. The presented model helps in the understanding of the underlying mechanisms that describe the dose rate sensitivity and the effect of hydrogen on dose rate effects. The model incorporates hole trapping mechanisms as well as the formation of interface traps due to the release of hydrogen as described by the two-stage hydrogen radiolysis model [10].

The model can be divided into two sets of key reactions that capture *dose rate effects* and *hydrogen effects*. A more complete set of equations is available upon request.

### 2.1 Dose Rate Effects

The mechanisms included in the model can be described by the following set of reactions between the mobile species and defects [11, 12]:

a) Hole trapping:

$$D_A + p \rightarrow D_A^+ \quad (1)$$

$$D_A^+ + n \rightarrow D_A \quad (2)$$

b) Proton Release:

$$D_BH + p \rightarrow D_BH^+ \quad (3)$$

$$D_BH^+ \rightarrow D_B + H^+ \quad (4)$$

$$D_BH^+ + n \rightarrow D_BH \quad (5)$$

c) Depassivation:

$$P_bH + H^+ \rightarrow P_b^+ + H_2 \quad (6)$$

Reactions (1) – (6) describe the mechanisms contributing to the radiation response following the generation of electron-hole pairs and initial "prompt" recombination. In (1) and (2) neutral hole trapping defects are denoted by $D_A$, and positively charged hole trapping defects are denoted by $D_A^+$. As described by reaction (2), a positively charged defect can be neutralized by capturing an electron. The formation of interface traps occurs through the "depassivation" of $P_b$-centers at the Si-$SiO_2$ interface. As described in the two-stage model [10], protons ($H^+$) are first released within the oxide and then migrate towards the interface, where they can react with the passivated dangling bond to form interface traps. It is commonly assumed that the proton is released following hole capture [14]. The first stage of the proton release model is described by reactions (3) – (5). In these reactions $D_BH$ is a hydrogenated neutral hole trapping defect. In the model, the atomic nature of $D_B$ is not determined. Reactions (3) and (4) describe proton release following hole capture. Reaction (5) describes electron capture at a positively charged hydrogenated defect (i.e., $D_BH^+$). *The competition between the mechanisms described by reactions* (*4*) *and* (*5*) *result in dose rate effects* [11]. In the second stage, protons that have reached the Si-$SiO_2$ interface can react with passivated $P_b$ centers ($P_bH$) as described by (6). The $P_bH$ centers are dangling bonds that have been passivated by hydrogen during processing—a reaction that will produce a dangling bond and release neutral hydrogen molecule (i.e., $H_2$).

Reactions are formulated into continuity equations describing the reactive transport for each mobile species. Following the notation in [6], the continuity equations are given by

$$\frac{dn_i}{dt} + \nabla \cdot \mathbf{J}_{si} = \sum_j \nu_{ij} R_j \,. \quad (7)$$

In (7), $n_i \equiv n_i(\mathbf{r},t)$ is the density for each species *i,* defined as a function of position $\mathbf{r}$ and time $t$, $\mathbf{J}_{si}$ is the species current density, $R_j$ is the reaction rate, and $\nu_{ij}$ is the stoichiometric coefficient giving the contribution from reaction $j$ to species $i$ [6]. The flux of each mobile species is given by $f_i = |\mathbf{J}_{si}|/q$. The kinetic equations describing the rates of the radiation-induced defects buildup are

$$\frac{dp_{t,A}}{dt} = \sigma_{pta} f_p N_{TA} - \sigma_{npta} f_n p_{t,A}, \tag{8}$$

$$\frac{dp_{t,B}}{dt} = \sigma_{ptb} f_p N_{TB} - \sigma_{nptb} f_n p_{t,B} - r_{pth} p_{t,B}, \tag{9}$$

$$\frac{dP_b}{dt} = \sigma_{it} f_{H^+} N_{P_bH}. \tag{10}$$

In (8) – (10), $N_{TA}$ and $N_{TB}$ are the density of hole traps (i.e., $D_A$) and the density of hydrogenated defects (i.e. $D_BH$); $p_{t,A}$ and $p_{t,B}$ are the density of trapped holes at hole traps and hydrogenated defects, respectively; $\sigma_{pta}$ and $\sigma_{ptb}$ are the captured cross-sections for holes at hole traps and at hydrogenated defects; $\sigma_{nptb}$ and $\sigma_{nptb}$ are the captured cross-sections for electrons at positively charged hole traps and at positively charged hydrogenated defects; $r_{pth}$ is the proton release coefficient from positively charged hydrogenated defects; $\sigma_{it}$ and $N_{P_bH}$ are the captured cross section for protons at passivated $P_b$ centers and the density of passivated $P_b$ centers at the Si-$SiO_2$ interface, respectively. The electrostatic potential ($\psi$) is obtained by solving Poisson's equation given by

$$\frac{\partial^2 \psi}{\partial x^2} = -\frac{\rho_{ox}}{\varepsilon_{ox}} = -\frac{q}{\varepsilon_{ox}} \left( p_{t,A} + p_{t,B} + n_{H^+} + p - n \right), \tag{11}$$

where all charged particles are included in the charge density term ($\rho_{ox}$).

A finite-difference methodology is used to compute solutions for the densities of the mobile species as well as for the electrostatic potential ($\psi$) at nodes contained within a mesh superimposed on the solution domain [15]. With this set of reactions, calculations for the buildup of $N_{it}$ can be plotted for any SiO2 system as a function of dose rate for a fixed total dose level.

## 2.2 Hydrogen Effects

To capture the effects of $H_2$ on dose rate response, the model follows the approach in [6], which adopts most of the formalisms presented by Stahlbush *et al*. and Mrstik *et al*. in [11-13]. In the model, hydrogen cracking occurs at positively charged defects. Therefore, $H_2$ disassociates to form hydrogenated defects (i.e., *DH* centers) by releasing a proton following hole capture (i.e., the positive charging of a defect). The $H_2$ cracking mechanisms are described by the following set of reactions [6]:

$\underline{H_2 \text{ cracking:}}$

$$D_C + p \rightleftarrows D_C^+ \tag{12}$$

$$D_C^+ + H_2 \rightleftarrows D_C H + H^+ \tag{13}$$

$$D_C H + p \rightarrow D_C H^+ \tag{14}$$

$$D_C H^+ \rightleftarrows D_C + H^+ \tag{15}$$

$$D_C^+ + n \rightarrow D_C \tag{16}$$

In reactions (12) – (15), a third kind of hole trapping defect is introduced, i.e., $D_C$. In the hydrogen cracking process, (12) describes hole capture resulting in positively charging the $D_C$ defect. Reaction (13) describes the cracking of $H_2$ at the positively charged defect, creating a DH center ($D_CH$) and releasing a proton. The resulting DH center can release additional protons as described by (14) and (15). Reaction (16) describes electron compensation at positively charged $D_C$ defects. In this case, dose rate dependence

results from the competition of (13) and (16). By introducing the hydrogen cracking mechanisms into the calculations it is possible to describe the effect of $H_2$ on the buildup of interface traps and on the dose rate response. The section below will describe the experimental results from irradiation performed on FOXFET and GLPNP devices. In the third section we will use the model to explain the results and draw conclusions about the key mechanisms responsible for the difference of degradation between devices.

## 3.0 EXPERIMENTAL RESULTS

### 3.1 FOXFETs

N-well-to-n-well (NW) FOXFETs were fabricated with 90-nm commercial bulk CMOS low-standby power (LSP) technology using STI oxides with a thickness of $t_{ox} \approx 425$ nm. FOXFET devices were fabricated with two 100-µm fingers (effective width is W = 200 µm) with poly-Si gate lengths of L = 1.5 µm. The test structures were irradiated with $^{60}$Co gamma rays at two different dose rates, 0.005 rad(Si)/s and 100 rad(Si)/s. During irradiation, the FOXFETs were biased with 1 V on the gate and all other terminals grounded. The thickness of the FOXFET oxide is greater than 400 nm, thus the field in the dielectric is still relatively low (< 25 kV/cm)—even with the 1 V bias on the gate.

Electrical measurements were performed prior to irradiation and following step-stress exposures to total dose levels of 3, 5, 10, 13.7 and 22.2 krad(Si) for the LDR experiments and 12 and 21 krad(Si) for the HDR experiments. The electrical measurements consisted of measuring the $I_d$ vs $V_{gs}$ characteristics for a drain bias of $V_d$ = 100 mV. The results for the LDR exposure are shown in Fig. 1. The results displayed in Fig. 2 are for an HDR exposure.

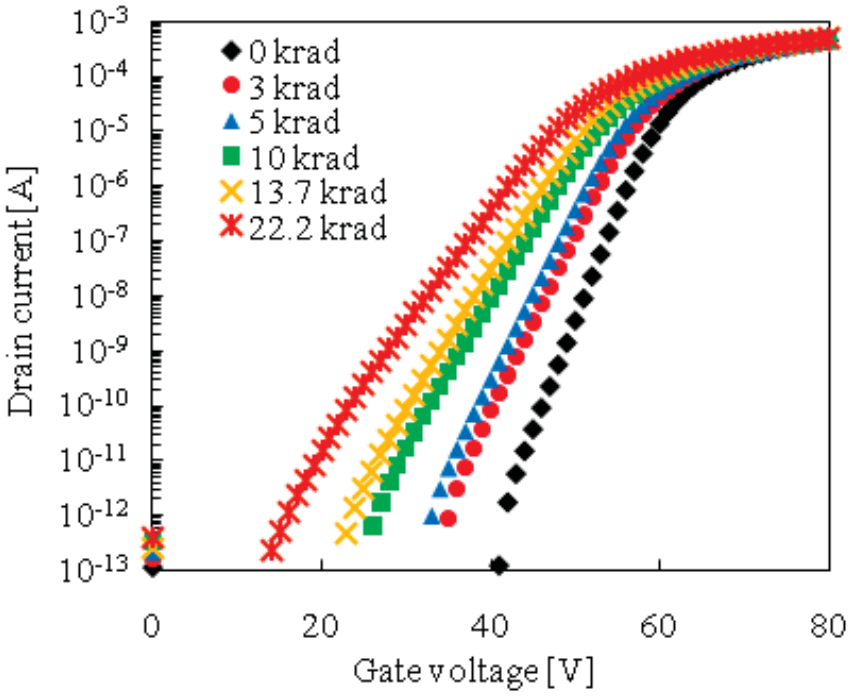


**Fig. 1**. $I_d$-$V_{gs}$ characteristics before irradiation and after 3, 5, 10, 13.7 and 22.2 krad(Si) of TID for NW FOXFET with W = 200 µ= 2L = 1.5 µ= 1Vd = 0.1 V, Vs = Vb = 0 V. Radiation bias was Vg = 1 V with all other terminals grounded. These results are for exposure at an LDR of 0.005 rad(Si)/s.

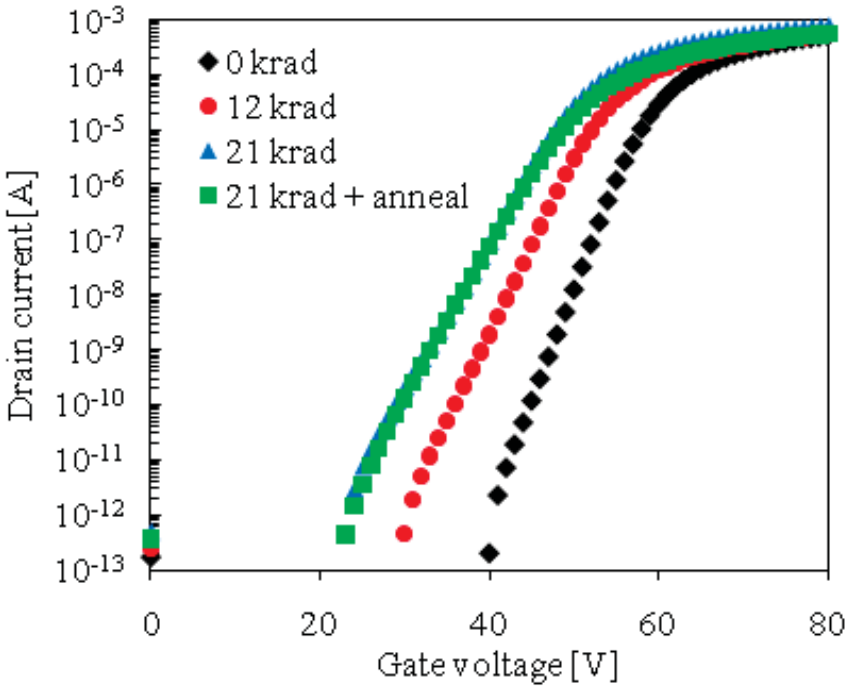


**Fig. 2**. $I_d$-$V_{gs}$ characteristics before irradiation and after 12 and 21 krad(Si) of TID for NW FOXFET with W = 200 μ= 2L = 1.5 μ= 1Vd = 0.1 V, Vs = Vb = 0 V. Radiation bias was Vg = 1 V with all other terminals grounded. These results are for exposure at an HDR of 100 rad(Si)/s.

The buildup of the effective oxide sheet-charge density ($\Delta N_{ot}$) and interface trap density ($\Delta N_{it}$) is extracted from the degraded I-V characteristics using the charge separation technique [16]. Shown in Fig. 3 are the extracted values of ($\Delta N_{ot}$ and ($\Delta N_{it}$) plotted as a function of dose for the LDR and the HDR experiments, respectively. The extractions for the LDR case are obtained from an average of two devices, while the HDR extractions are from a single device. Following HDR exposure, devices were annealed at room temperature with the same biasing configuration (i.e., $V_g$ = 1 V with all other terminals grounded). The annealing time is determined by the time required to reach the total dose level (21 krad in this case) at the LDR exposure. This ensures the same amount of time is allowed for the transport of mobile species in both the LDR and HDR cases and, thus, the "true" dose rate effects are measured. True dose rate effects are determined by comparing the radiation response of devices exposed at an LDR and devices exposed at an HDR followed by a room temperature anneal. The results in Fig. 3 show a greater buildup in both $N_{ot}$ and $N_{it}$ following the LDR exposures than following an HDR exposure with the corresponding room temperature anneal. These results indicate that there is an LDR to HDR enhancement factor (EF) of approximately 1.3 for $N_{ot}$ and approximately 1.6 for $N_{it}$. In comparison, the damage EF for bipolar technologies can be as high as ~ 2 for $\Delta N_{ot}$ and up to 10 or greater for $\Delta N_{it}$ [8, 17]. Additional experiments were performed with all terminals grounded during irradiation (results not shown). The results from both radiation biasing configurations (i.e., 1 V on the gate and 0 V on the gate, with all other terminals grounded) indicate a similar buildup rate for $N_{ot}$ and $N_{it}$.

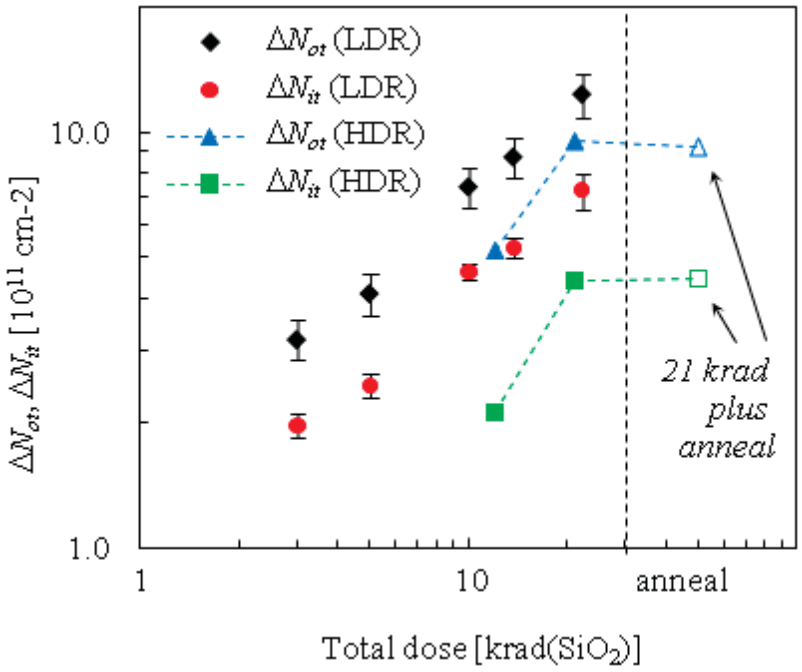


**Fig. 3.** $\Delta N_{ot}$ and $\Delta N_{it}$ plotted as a function of total dose. Values are extracted from FOXFETs with $W$ = 200 μm and $L$ = 1.5 μm exposed at 0.005 rad($SiO_2$)/s (LDR) and at 100 rad($SiO_2$)/s (HDR) using a 1 V bias on the gate during irradiation.

### 3.2 GLPNP

GLPNP transistors fabricated using the National Semiconductor Corporation (NSC) linear bipolar circuit technology were used to investigate the effects of $H_2$ concentration on the buildup of $N_{it}$. The base oxides in these devices have a thickness of 1.22 μm and consist of a thermal oxide covered by a deposited oxide that is used to assure adequate oxide thickness over the emitter [15]. These GLPNP transistors are the same test structures used in [18, 19] to obtain the $\Delta N_{it}$ plotted in Fig. 4.

This plot illustrates the change in $\Delta N_{it}$ as a function of dose rate for irradiation in three different ambient hydrogen conditions, 0% (i.e., in air), 1% $H_2$ and 100% $H_2$ after a $^{60}$Co total dose exposure of 30 krad(Si). It indicates that the devices exposed in air show a typical dose rate curve with an enhanced buildup of $N_{it}$ at the low dose rates (LDR). In this case, the transition from the high dose rate (HDR) asymptote to greater values of $\Delta N_{it}$ at LDR occurs at ~ 1 rad(Si)/s. As the hydrogen concentration increases, the transition dose rate shifts to the right and $\Delta N_{it}$ appears to increases at the HDR and LDR limits. However, these hypothetical fitting curve at a lower dose rate needed to be confirmed with additional experiments to investigate the enhancement of $\Delta N_{it}$ in the presence of $H_2$ at a lower dose rate; i.e., 0.005 rad(Si)/s.

LDR irradiations were done at the Jet Propulsion Laboratory (JPL) with $^{60}$Co gamma rays at a dose rate of 0.005 rad(Si)/s in an environment containing different concentrations of $H_2$ (i.e., 0%, 1% and 100%) with the same procedure described in [18]. For the case of HDR irradiations, the GLPNP test structures were only irradiated in air (i.e., 0% $H_2$). Electrical characterization was performed prior to irradiation and following step-stress exposures to total dose levels of 10, 20 and 30 krad(Si), with all terminals grounded during irradiation. The buildup of interface trap density ($\Delta N_{it}$) is extracted from the degraded I-V characteristics using the technique described in [16]. Shown in Fig. 5 are the extracted values of $\Delta N_{it}$ plotted as a function of total dose for HDR and LDR exposures in three different ambient hydrogen conditions. The extractions are obtained from an average of two devices and the error bars represent one standard deviation. Following HDR exposure, devices were annealed at room temperature with the same

biasing configuration (i.e., all terminals grounded). True dose rate effects are measured by comparing the radiation response of devices exposed at an LDR and devices exposed at an HDR followed by a room temperature anneal. This makes it possible to differentiate time-dependent effects from true dose rate effects. The annealing time is determined by the time required to reach 30 krad(Si) at the LDR exposure.

The results shown in Fig. 5 indicate that there is an enhancement in the buildup of $N_{it}$ for devices exposed to LDR as compared to HDR followed with room temperature anneal. The enhancement factor at 30 krad(Si) is approximately 4.8 and is consistent with the results in Fig. 1. However, the results also indicate that the enhancement in degradation due to $H_2$ concentration saturates at the low dose rate of 0.005 rad(Si)/s. This is evident in the results shown in Fig. 5, where the extractions of $\Delta N_{it}$ for devices exposed at LDR in all different ambient hydrogen conditions are considerably similar. These results are somewhat different from the results presented by Pease et al. [18], which showed no saturation for LDR irradiations (below 0.005 rads/s) of the National Semiconductor Corporation (NSC) LM193 dual voltage comparator at different concentrations of $H_2$.

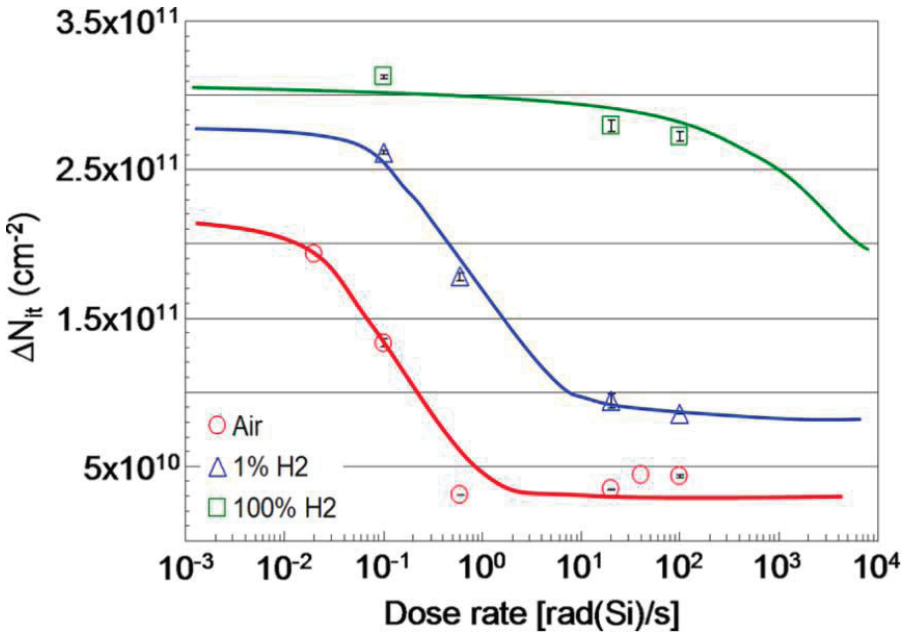


**Fig. 4**. Buildup of interface trap density ($\Delta N_{it}$) in GLPNP bipolar devices as a function of dose rate for irradiation in three different ambient hydrogen conditions at a total dose of 30 krad(Si) [17, 18].

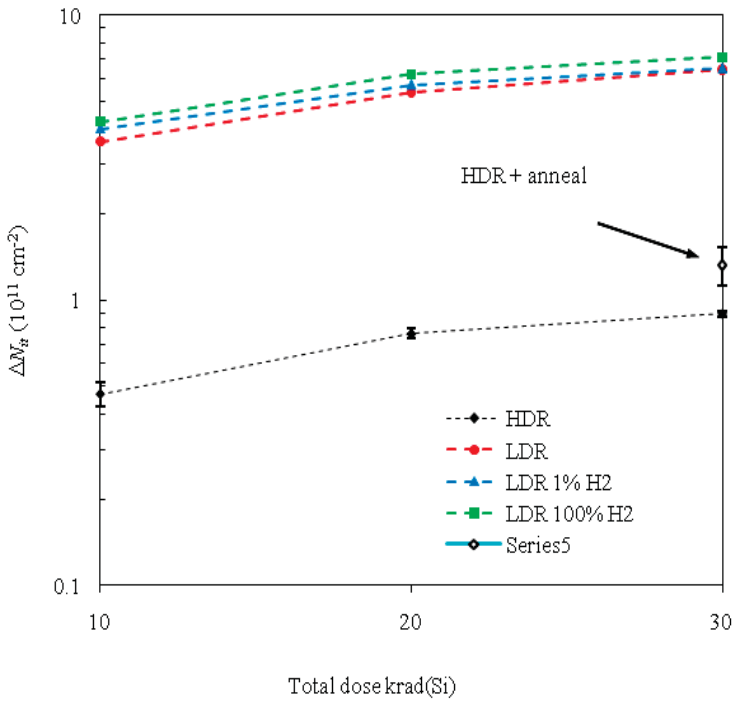


**Fig. 5**. Buildup of interface trap density ($\Delta N_{it}$) in GLPNP bipolar devices as a function of total dose. LDR exposures were done in three different ambient hydrogen conditions (0%, 1% and 100% $H_2$). Open symbol is the value of $\Delta N_{it}$ extracted after HDR exposure and room temperature anneal. LDR = 0.005 rad(Si)/s, HDR = 100 rad(Si)/s.

## 4.0 CALCULATIONS

To explain the results from experiments obtained using irradiation on both FOXFET and GLPNP devices, we use the 1-D model described in section 2.0. We used a finite-difference methodology for the numerical calculations. This computes solutions for the densities of the mobile species and for the electrostatic potential at nodes contained within a mesh superimposed on the solution domain [19]. These calculations allow for studying the key mechanisms responsible for differences in enhancement factor (EF) between devices as well as identifying the key mechanisms responsible for the build-up of $N_{it}$ at low dose rate and in presence of molecular hydrogen.

### 4.1 Calculation 1: Dose Rate Effects

The first set of calculations, shown in Fig. 6, plots the buildup of $N_{it}$ as a function of dose rate at a total dose of 30 krad($SiO_2$) for different values of $t_{ox}$. All of the calculations in Fig. 5 are obtained from *transient simulations* performed up to a maximum total time of $3\times10^7$ s, which is the time required to reach a dose of 30 krad($SiO_2$) at the lowest dose rate. These calculations are obtained using a uniform density of hydrogenated defects, $N_{TB} = 10^{15}$ $cm^{-3}$, distributed throughout the oxide, and a uniform density of hole traps, $N_{TA} = 10^{19}$ $cm^{-3}$, located within 25 nm of the Si-$SiO_2$ interface. Other model parameters used in the calculations are given in Table II. The defect densities and capture cross sections used here are consistent with values reported in [4, 17, 6, 20, 21, 22]. The results plotted in Fig. 5 show that at low dose rates, the buildup of $N_{it}$ is suppressed as $t_{ox}$ and is reduced from 1000 nm to 400 nm (i.e., $\Delta N_{it}$ is lower for $t_{ox}$ = 400 nm for dose rates below 0.1 rad($SiO_2$)/s). This reduction is a result of fewer protons being released within the thinner oxides, as described by reaction (4), and consequently resulting in a lower $\Delta N_{it}$. For increasing dose rates, the competition between reactions (4) and (5) becomes more significant as the density of radiation-induced generated ehps becomes comparable to $N_{TB}$. In this case, electron recombination at $D_BH^+$ reduces the amount of protons being released within the oxide, resulting in a reduction in $\Delta N_{it}$ at higher dose rates. This neutralization process is described by reaction (5). However, the results in Fig. 6 show that the reduction in $\Delta N_{it}$ as a function of dose rate (i.e., the dose rate sensitivity) is more significant for $t_{ox}$ = 1000 nm than for $t_{ox}$ = 400 nm. The LDR to HDR EF is reduced from approximately 6.2 for $t_{ox}$ = 1000 nm to approximately 1.8 for $t_{ox}$ = 400 nm. The EF is obtained from the ratio of $\Delta N_{it}$ for dose rates of $10^{-3}$ rad($SiO_2$)/s and $10^2$ rad($SiO_2$)/s. The difference in dose rate sensitivity as a function of $t_{ox}$ can be explained by space charge effects.

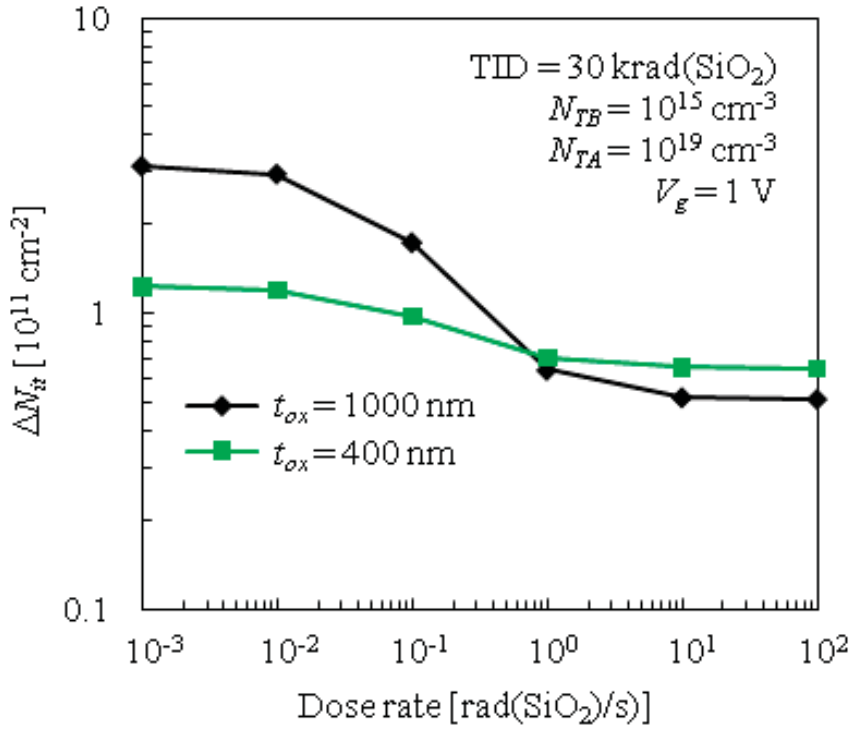


**Fig. 6**. Calculations for the buildup of $N_{it}$ plotted as a function dose rate for a total dose of 30 krad(Si) and for different values of $t_{ox}$.

TABLE II
SIMULATION INPUT PARAMETERS FOR
CALCULATIONS IN FIGS. 5 AND 6

| Parameter | Value | Units |
|---|---|---|
| $N_{P_bH}$ | $10^{13}$ | cm$^{-2}$ |
| $\sigma_{pta}$ | $5.5\times10^{-14}$ | cm$^2$ |
| $\sigma_{ptb}$ | $5.5\times10^{-14}$ | cm$^2$ |
| $\sigma_{npta}$ | $5.0\times10^{-13}$ | cm$^2$ |
| $\sigma_{nptb}$ | $2.0\times10^{-12}$ | cm$^2$ |
| $\sigma_{it}$ | $10^{-11}$ | cm$^2$ |
| $r_{pth}$ | $10^{-5}$ | s$^{-1}$ |

Space charge effects that contribute to dose rate sensitivity are investigated by using different densities of hole trapping defects (i.e., $N_{TA}$). A higher $N_{TA}$ results in more fixed positive charge near the Si-SiO$_2$ interface. Localized electric fields caused by the fixed positive charge and other radiation-generated

species can result in the confinement of electrons within the oxide bulk [2, 3]. The confinement of electrons enhances recombination at $D_BH^+$ sites, and contributes to dose rate sensitivity. Shown in Fig. 7 is a plot of the EF obtained by the ratio of $\Delta N_{it}$ at a total dose of 30 krad(Si) for dose rates of $10^{-3}$ rad(Si)/s and $10^3$ rad(Si)/s. The EF is plotted as a function of $t_{ox}$ for two different densities of hole traps, $N_{TA} = 10^{19}$ $cm^{-3}$ and $10^{18}$ $cm^{-3}$, located within 25 nm of the Si-$SiO_2$ interface. The results in Fig. 6 show that *a higher density of hole trapping defects near the Si-$SiO_2$ interface enhances dose rate sensitivity as a function of oxide thickness*. Space charge effects are due to localized electric fields caused by radiation-generated species and can alter the transport of charged particles during irradiation. However, as $t_{ox}$ is reduced, space charge effects become less significant since the transport of charged particles is predominantly determined by the electric field set by the gate bias and the gate-to-semiconductor work function difference. This effect is demonstrated by the calculation results shown in Fig. 7. Here, for the case of $N_{TA} = 10^{19}$ $cm^{-3}$, dose rate sensitivity is significantly impacted by oxide thickness as determined by the increase in EF as a function of $t_{ox}$. On the other hand, for $N_{TA} = 10^{18}$ $cm^{-3}$, the impact of $t_{ox}$ on dose rate sensitivity is less significant as determined by the nearly constant EF as a function of $t_{ox}$.

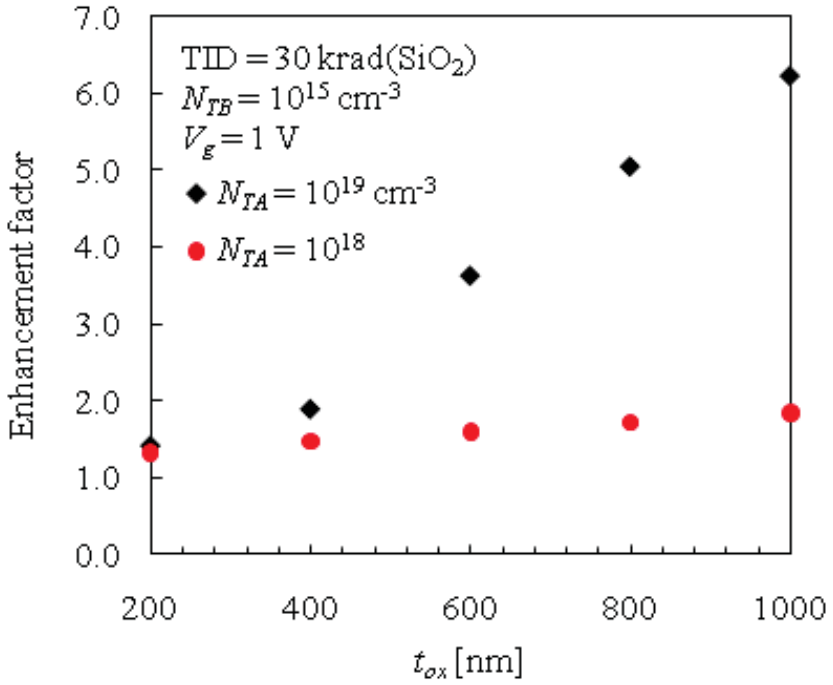


Fig 7. LDR to HDR enhancement factor given by the ratio of $N_{it}$ for dose rates of $10^{-3}$ rad(Si)/s and $10^3$ rad(Si)/s plotted as a function of $t_{ox}$, for two different densities of hole traps, NTA = $10^{19}$ $cm^{-3}$ and $10^{18}$ $cm^{-3}$, located within 25 nm of the Si-$SiO_2$ interface. For these calculations NTB = $10^{15}$ $cm^{-3}$ and is uniformly distributed in the oxide.

Additional data from numerical calculation are shown in Fig. 8. Data show a plot of the LDR to HDR enhancement factor calculated by the ratio of $N_{it}$ at a total dose of 30 krad(Si) for dose rates of $10^{-3}$ rad(Si)/s and 100 rad(Si)/s. The enhancement factor is plotted as a function of the electron capture cross section at positively charged hydrogenated defects (i.e., $\sigma_{nptb}$) and for two different densities of hole traps, $N_{TA} = 10^{19}$ $cm^{-3}$ and $10^{18}$ $cm^{-3}$, located within 25 nm of the Si-$SiO_2$ interface. For the lower values of $\sigma_{nptb}$, electron compensation at positively charged hydrogenated defects, i.e., reaction (5) is not significant. Consequently, the enhancement factor, and therefore dose rate sensitivity, is independent of electron compensation at positively charged hydrogenated defects for values below $10^{-13}$ $cm^2$. For these values of

$\sigma_{nptb}$, the simulated enhancement factor is simply the result of space charge effects that arise from buildup of fixed positive charge at hole traps near the Si-$SiO_2$ interface and thus increases with NTA. For $\sigma_{nptb}$ = $10^{-14}$ $cm^2$ the enhancement factor is ~1 for NTA = $10^{18}$ $cm^{-3}$and ~3.5 for NTA = $10^{19}$ $cm^{-3}$. As $\sigma_{nptb}$ increases above $10^{-13}$ $cm^2$, the enhancement factor increases as the reaction between electrons and $D_BH+$ centers becomes more significant at higher dose rates. However, the enhancement is greater for the case of NTA = $10^{19}$ $cm^{-3}$ since space charge confines electrons in the oxide bulk, allowing more recombination to occur. A higher NTA results in more fixed positive charge near the Si-$SiO_2$ interface and therefore more confinement of electrons in the oxide bulk.

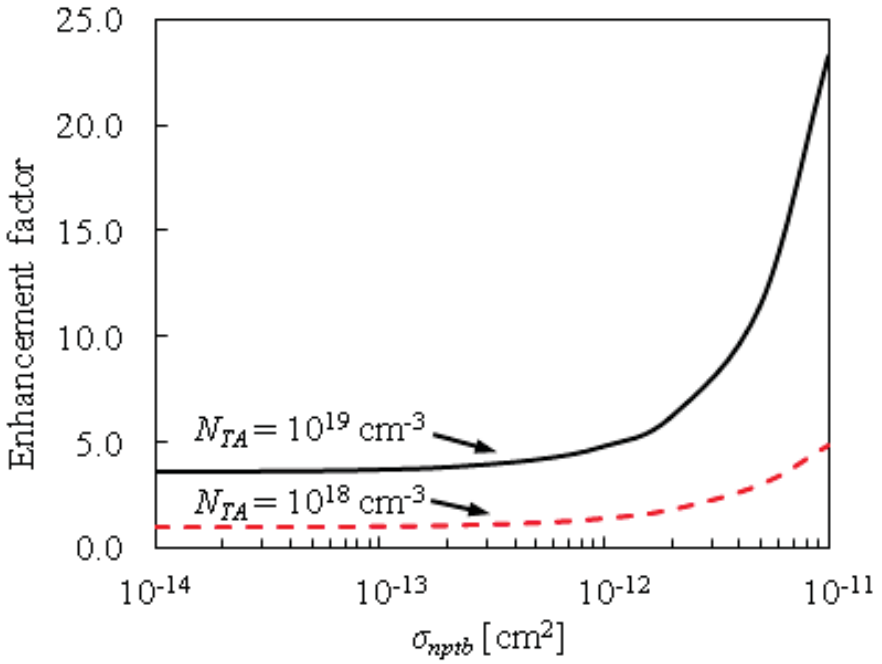


Fig. 8. LDR to HDR enhancement factor obtained by the ratio of $N_{it}$ for dose rates of $10^{-3}$ rad(Si)/s and 100 rad(Si)/s for two different densities of hole traps, NTA = 1019 $cm^{-3}$ and 1018 $cm^{-3}$, located within 25 nm of the Si-SiO2 interface. For these calculations NTB = 1016 $cm^{-3}$ and is uniformly distributed in the oxide.

## 4.2 Calculation 2: Effect of Hydrogen

We performed additional calculations to study the impact of hydrogen on the total dose and dose rate response using the 1-D model on a MOS structure that simulates the gated base oxide region of the GLPNP bipolar transistors. The simulation parameters include a fixed gate work-function, uniform Si substrate doping concentration and a base oxide thickness of 1.22 μm. Other parameters are the same as listed in Table I, except $N_{TC}$ = $10^{15}$ $cm^{-3}$, which is the density of defects $D_C$. For these calculations no initial density of hydrogenated defects is specified (i.e., $N_{TB}$ = 0). Shown in Fig. 9 are the model calculations of $N_{it}$ plotted as a function of dose rate for three different concentrations of $H_2$. The results in Fig. 9 shows a shift to the right in the dose rate response of $N_{it}$ (i.e., the $N_{it}$ vs dose rate curve) as the concentration of $H_2$ is increased. This shift is consistent with the experimental data shown in Fig. 4. As mentioned above, dose rate effects arise from the competing contributions of reactions (13) and (16). Increasing the concentration of $H_2$ favors reaction (13), resulting in more protons being released. Therefore, the dose rate response is shifted to right as a greater density of electrons is required for recombination mechanisms to become significant.

It should be noted that the saturation point can be controlled depending on the oxide parameters, indicating that by using a known oxide process, it would be possible to predict the expected enhancement factor for a specific device at a specific dose for a low dose rate conditions. As a result, it is not surprising that we see saturation for the GLPNP devices and no saturation for the LM193 dual-comparator from NSC reported by Pease [18].

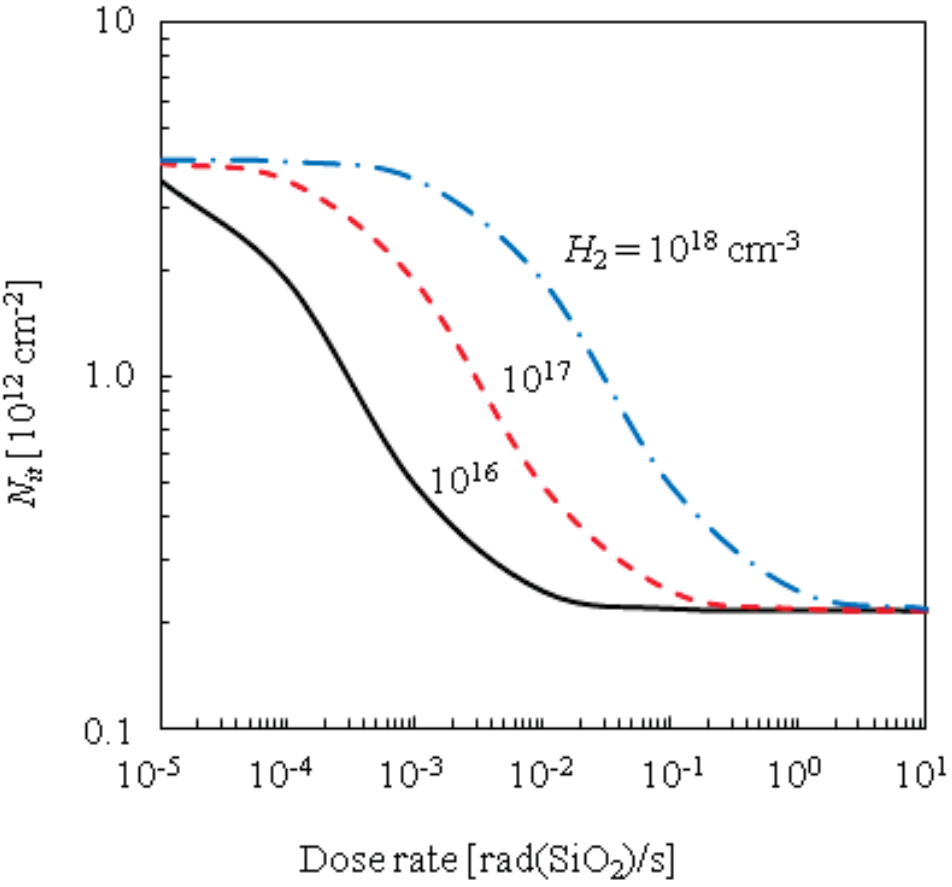


Fig. 9. Calculations of $N_{it}$ plotted as a function of dose rate for three different concentrations of $H_2$.

### 4.3 Calculation 3: Comparison Between STI Deposited Oxides vs Thermal Oxides

Fig. 10 plots the buildup of interface trap density as a function of dose rate for the FOXFET data shown in Fig. 3 and for data on gated-lateral pnp (GLPNP) transistors [18]. The FOXFET data corresponds to a total dose of 21 krad($SiO_2$) and the GLPNP transistor data corresponds to a total dose of 30 krad($SiO_2$). $\Delta N_{it}$ for the GLPNP transistors is extracted using the methods discussed in [23, 24]. Degradation in the GLPNP transistors is a result of interface trap buildup at the base oxide-silicon interface. The base oxide thickness for the GLPNP transistors is $t_{ox}$ = 1.22 μm. As described in the previous section, oxide thickness and the density of hole traps (i.e., NTA) can affect dose rate sensitivity. However, trapping properties that result from different oxide processing may also affect dose rate sensitivity. For example, as reported in [25], most of the hole trapping in thermal oxides occurs near the Si-$SiO_2$ interface, whereas deposited oxides can have a significant amount of hole trapping deeper within the bulk. Additionally, the capture cross section for hole traps (i.e., $\sigma_{pta}$) appears to be smaller in deposited oxides than in thermal oxides [25]. The GLPNP base oxide consists of a thermally grown oxide covered by a deposited oxide that is used to assure adequate oxide thickness over the emitter [24]. For STI oxides, typical processing

involves etching a trench pattern through a nitride layer, sidewall oxidation to grow a thin oxide liner, chemical vapor deposition to fill the trench and chemical-mechanical planarization polishing [25]. Therefore, the bulk of the STI will consist of a deposited oxide.

Additional calculations were to investigate how the differences in oxide processing between base oxides in GLPNP transistors and STI oxides in FOXFETs affect the dose rate sensitivity. The solid and dashed lines in Fig. 10 correspond to these calculations. The calculations fitted to the GLPNP transistor data (i.e., the solid line) are obtained using a uniform density of hydrogenated defects, $N_{TB}$ = 8.5×1014 $cm^{-3}$, distributed throughout the oxide and a uniform density of hole traps, $N_{TA}$ = 1019 $cm^{-3}$, located within 25 nm of the Si-$SiO_2$ interface. All other parameters are the same as listed in Table I. For the case of the FOXFETs, the calculations are fitted using $N_{TB} = 6.5\times10^{15}$ $cm^{-3}$ distributed uniformly throughout the oxide and NTA = $10^{19}$ $cm^{-3}$ located within 75 nm of the Si-$SiO_2$ interface (dashed line in Fig. 10). In this case, all other parameters are the same as listed in Table I except hole capture cross section, which is reduced to $\sigma_{pta} = 5.5\times10^{-15}$ $cm^2$. Calculations show that increasing the depth within the oxide where hole traps are located (as measured from the Si-$SiO_2$ interface) slightly increases dose rate sensitivity. However, the reduction in hole capture cross section reduces the buildup of fixed positive charge near the Si-$SiO_2$ interface, significantly reducing dose rate sensitivity. This results in a better agreement with the FOXFET data.

The impact of hole capture cross section on dose rate sensitivity can be observed in the calculations shown in Fig. 11 where EF is plotted as a function of $\sigma_{pta}$. EF is obtained from the ratio of $\Delta N_{it}$ for dose rates of $10^{-3}$ rad (Si)/s and $10^{3}$ rad(Si)/s. The results in Fig. 11 show that for a fixed location and density of hole traps (e.g., NTA = $10^{19}$ $cm^{-3}$ located within 25 nm of the Si-$SiO_2$ interface) the dose rate sensitivity is independent of $\sigma_{pta}$ for values below ~$4\times10^{-14}$ $cm^2$. However, as $\sigma_{pta}$ increases, significant hole trapping in regions near the Si-$SiO_2$ interface increases dose rate sensitivity as determined by the increased EF obtained for values above ~$4\times10^{-14}$ $cm^2$. The calculations also show that the value for $\sigma_{pta}$ where the transition in dose rate sensitivity occurs is reduced by extending the location of the hole traps from within 25 nm of the Si-$SiO_2$ interface to 45 nm.

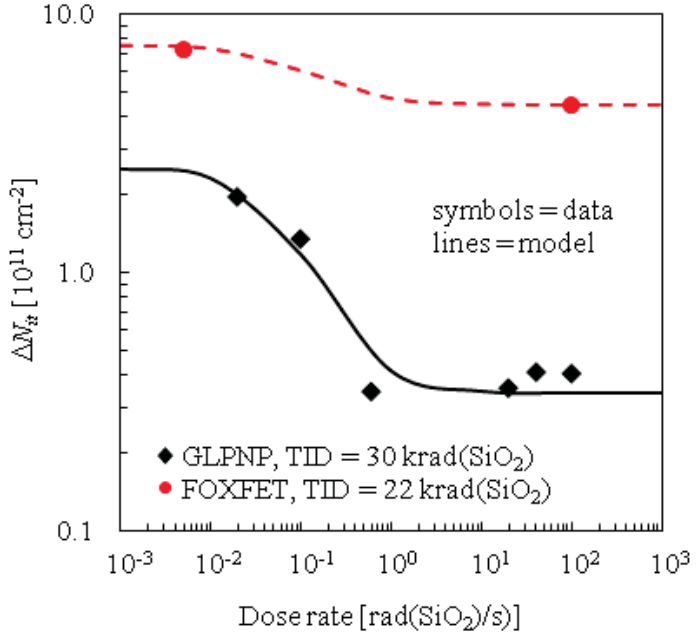


Fig. 10. $\Delta N_{it}$ plotted as a function of dose rate for the FOXFETs (from data in Fig. 4) and for GLPNP transistors fabricated in the National Semiconductor Corporation (NSC) linear bipolar circuit technology. FOXFET data corresponds to a total dose of 21 krad($SiO_2$) and the GLPNP transistor data corresponds to a total dose of 30 krad($SiO_2$). Symbols indicate data and solid lines model calculations.

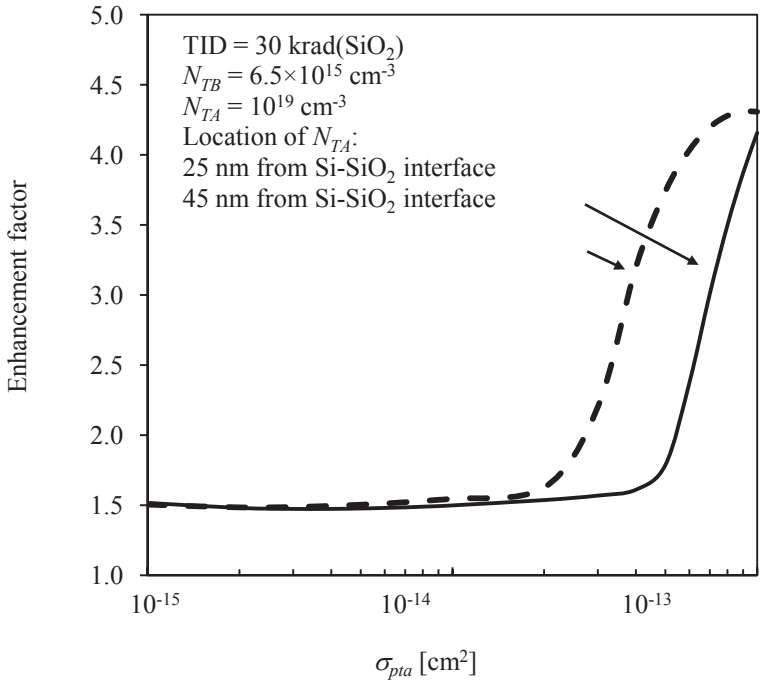


Fig. 11. Enhancement factor in the buildup of interface trap density obtained by the ratio of $\Delta N_{it}$ at a dose rate of $10^{-3}$ rad(Si)/s to $\Delta N_{it}$ at a dose rate and $10^{3}$ rad(Si)/s plotted as a function of the hole capture cross section ($\sigma_{pta}$). The solid lines are calculations for NTA located within 25 nm of the Si-$SiO_2$ interface and dashed lined for NTA located within 45 nm of the interface.

## 5.0 DISCUSSION AND CONCLUSIONS

The impact of different model parameters on the dose rate dependent buildup of interface traps can be investigated using the numerical calculations described in Section 2. This analysis makes it possible to understand how differences in technological and processing characteristics between bipolar base oxides and advanced CMOS STI oxides result in different dose rate sensitivities. From the model calculations, it has been determined that oxide thickness, the density and location of hole traps, and hole capture cross-section all affect dose rate sensitivity. The density and location of hole traps, as well as the hole capture cross section, affect the buildup of fixed charge near the $Si\text{-}SiO_2$ interface, which can result in space charge effects that enhance recombination mechanisms and impact the dose rate sensitivity. The numerical calculations presented indicate that dose rate sensitivity can result from the combined effects of space charge and recombination mechanisms. However, the contribution from space charge effects becomes less significant as $t_{ox}$ is reduced because the transport of charged particles during irradiation is determined by the electric field set by the gate bias and the gate-to-semiconductor work-function difference.

Comparison of model calculations with experimental data results in excellent agreement for the description of dose rate sensitivity. The difference in dose rate sensitivity between base oxides of bipolar devices and advanced CMOS STI oxides is captured through differences in oxide thickness, in the location of hole traps (i.e., the location of $N_{TA}$) and in the value of hole capture cross section. The differences in the location of $N_{TA}$, and in the values of $\sigma_{pta}$ are consistent with observations made by Mrstik *et al*. in [25] based on experimental characterization of deposited oxides using photo-assisted injection techniques.

Other model parameters such as electron capture cross-section at positively charged hydrogenated defects (i.e., $\sigma_{nptb}$) and proton release coefficient from positively charged hydrogenated defects (i.e., $r_{pth}$) can also impact dose rate sensitivity. As described in [24], important factors that impact dose rate sensitivity in bipolar technologies are final passivation, packaging and post-packaging thermal treatments and hydrogen contamination in the package. However, the work presented here provides strong evidence that specific technology and processing characteristics of isolation oxides can explain the differences observed in dose rate sensitivity between bipolar and CMOS technologies.

In addition, with respect to the hydrogen contamination issue, results in Fig. 9 demonstrate good qualitative agreement between the analytical model and the experimental data shown in Fig. 4, particularly in the transition region between high and low dose rate responses. At present, the model does not capture the impact of hydrogen on the HDR and LDR asymptotes. One explanation for the increase in interface trap buildup at the low and high dose rate extremes is that hydrogen alters the density of precursor species and other reactants. However, as observed in Fig. 9, saturation in the enhancement of $\Delta N_{it}$ at LDR in the presence of $H_2$ occurs in some cases. A contributing factor to the differences in saturation of $\Delta N_{it}$ as measured at LDR may be the different concentrations of molecular hydrogen and hole trapping defects (i.e., $N_{TC}$) in oxide regions for a given hydrogen ambient condition. Experimental results and model calculations indicate that saturation of $\Delta N_{it}$ in the presence of hydrogen for devices exposed at LDR may vary based on the trapping characteristics and concentration of $H_2$ in the oxide.

## 6.0 REFERENCE


[1] E. W. Enlow, R. L. Pease, W. Combs, R. D. Schrimpf, and R. N. Nowlin, “Response of advanced bipolar processes to ionizing radiation,” IEEE Trans. Nucl. Sci., vol. 38, pp. 1342-1351, 1991.

[2] D. M. Fleetwood, S. L. Kosier, R. N. Nowlin, R. D. Schrimpf, R. A. Reber, Jr., M. DeLaus, P. S. Winokur, A. Wei, W. E. Combs, and R. L. Pease, “Physical mechanisms contributing to enhanced bipolar gain degradation at low dose rates,” IEEE Trans. Nucl. Sci., vol. 41, pp. 1871-1883, 1994.

[3] D. M. Fleetwood, L. C. Riewe, J. R. Schwank, S. C. Witczak and R. D. Schrimpf, “Radiation effects at low electric fields in thermal, SIMOX, and bipolar-base oxides,” IEEE Trans. Nucl. Sci., vol.43, no.6, pp.2537-2546, 1996.

[4] S. N. Rashkeev, C. R. Cirba, D. M. Fleetwood, R. D. Schrimpf, S. C. Witczak, A. Michez, and S. T. Pantelides, “Physical model for enhanced interface-trap formation at low dose rates,” IEEE Trans. Nucl. Sci., vol. 49, pp. 2650-2655, 2002.

[5] H. P. Hjalmarson, R. L. Pease, S. C. Witczak, M. R. Shaneyfelt, J. R. Schwank, A. H. Edwards, C. E. Hembree, and T. R. Mattsson, “Mechanisms for radiation dose-rate sensitivity of bipolar transistors,” IEEE Trans. Nucl. Sci., vol. 50, pp. 1901-1909, 2003.

[6] H. P. Hjalmarson, R. L. Pease, and R. A. B. Devine, “Calculations of Radiation Dose-Rate Sensitivity of Bipolar Transistors,” IEEE Trans. Nucl. Sci., vol. 55, pp. 3009-3015, 2008.

[7] D. M. Fleetwood, P. S. Winokur, and J. R. Schwank, “Using laboratory x-ray and cobalt-60 irradiations to predict CMOS device response in strategic and space environments,” IEEE Trans. on Nucl. Sci. Vol. 35, No. 6, pp.1487-1505, 1988.

[8] A. H. Johnston, R. T. Swimm, and T. F. Miyahira, “Low Dose Rate Effects in Shallow Trench Isolation Regions,” IEEE Trans. on Nucl. Sci. Vol. 57, No. 6, pp. 3279-3287, 2010.

[9] S. C. Witczak, R. C. Lacoe, J. V. Osborn, J. M. Hutson, and S. C. Moss, “Dose-rate sensitivity of modern nMOSFETs," IEEE Trans. on Nucl. Sci. Vol. 52, No. 6, pp. 2602-2608, 2005.

[10] F. B. McLean, "A Framework for Understanding Radiation-Induced Interface States in SiO2 MOS Structures," IEEE Trans. Nucl. Sci., vol. 27, pp. 1651-1657, 1980.

[11] R. E. Stahlbush, A. H. Edwards, D. L. Griscom, and B. J. Mrstik, "Post-irradiation cracking of H2 and formation of interface states in irradiated metal-oxide-semiconductor field-effect transistors," J. Appl. Phys., vol. 73, pp. 658-667, 1993.

[12] B. J. Mrstik and R. W. Rendell, “Si-SiO2 interface state generation during X-ray irradiation and during post-irradiation exposure to a hydrogen ambient [MOSFET],” IEEE Trans. Nucl. Sci., vol. 38, pp. 1101-1110, 1991.

[13] R. E. Stahlbush, B. J. Mrstik, and R. K. Lawrence, “Post-irradiation behavior of the interface state density and the trapped positive charge,” IEEE Trans. Nucl. Sci., vol. 37, pp. 1641-1649, 1990.

[14] M. R. Shaneyfelt, J. R. Schwank, D. M. Fleetwood, P. S. Winokur, K. L. Hughes and F. W. Sexton, "Field dependence of interface-trap buildup in polysilicon and metal gate MOS devices," IEEE Trans. Nucl. Sci., vol. 37, pp. 1632-1640, 1990.

[15] C. M. Snowden, Introduction to Semiconductor Device Modeling: World Scientific, 1986.

[16] P. S. Winokur, J. R. Schwank, P. J. McWhorter, P. V. Dressendorfer, and D. C. Turpin, "Correlating the radiation response of MOS capacitors and transistors," IEEE Trans. Nucl. Sci., vol. 31, pp. 1453-1460, 1984.

[17] X. J. Chen, H. J. Barnaby, P. Adell, R. L. Pease, B. Vermeire, and K. E. Holbert, "Modeling the dose rate response and the effects of hydrogen in bipolar technologies," IEEE Trans. Nucl. Sci., vol. 56, pp. 3196-3202, 2009.

[18] R. L. Pease, P. C. Adell, B. G.Rax, X. J. Chen, H. J.Barnaby, K. E. Holbert and H. P. Hjalmarson, “The Effects of Hydrogen on the Enhanced Low Dose Rate Sensitivity (ELDRS) of Bipolar Linear Circuits,” IEEE Trans. Nucl. Sci., vol.55, no.6, pp.3169-3173, Dec. 2008

[19] Radiation Effects Module User's Manual, 5.9.31.C ed. Santa Clara: Silvaco International, 2005.

[20] F. B. McLean, "A framework for understanding radiation-induced interface states in SiO2 MOS structures," IEEE Trans. Nucl. Sci., vol. 27, pp. 1651-1657, 1980.

[21] H. P. Hjalmarson, R. L. Pease, S. C. Witczak, M. R. Shaneyfelt, J. R. Schwank, A. H. Edwards, C. E. Hembree, and T. R. Mattsson, “Mechanisms for radiation dose-rate sensitivity of bipolar transistors,” IEEE Trans. Nucl. Sci., vol. 50, pp. 1901-1909, 2003.

[22] A. G. Revesz, “Chemical and structural aspects of the irradiation behavior of SiO films on silicon,” IEEE Trans. Nucl. Sci., vol. NS-24, p.2102, 1977.

[23] R. L. Pease, D. G. Platteter, G. W. Dunham, J. E. Seiler, H. J. Barnaby, R. D. Schrimpf, M. R. Shaneyfelt, M. C. Maher and R. N. Nowlin, “Characterization of enhanced low dose rate sensitivity (ELDRS) effects using gated lateral pnp transistor structures,” IEEE Trans. Nucl. Sci., vol. 51, pp. 3773-3780, 2004.

[24] B. J. Mrstik, H. L. Hughes, R. K. Lawrence, P. J. McMarr and P. Gouker, “Comparison of charge trapping in undoped oxides made by low- and high-temperature deposition techniques,” IEEE Trans. Nucl. Sci., vol. 48, pp. 2107-2113, 2001.

[25] C. F. Lin, W. T. Tseng, M. S. Feng, and Y. L. Wang, "A ULSI shallow trench isolation process through the integration of multilayered dielectric process and chemical-mechanical planarization," Thin Solid Films, vol. 347, pp. 248-252, 1999.